NeuroImage 55 (2011) 1373–1383

Contents lists available at ScienceDirect

NeuroImage

journal homepage: www.elsevier.com/locate/ynimg

Error-related medial frontal theta activity predicts cingulate-related structural connectivity

Michael X Cohen *

Department of Psychology, University of Amsterdam, Roetersstraat 15, 1018 WB, Amsterdam, The Netherlands
Department of Physiology, University of Arizona, Tucson, USA

ARTICLE INFO

Article history:
Received 21 September 2010
Revised 30 November 2010
Accepted 24 December 2010
Available online 31 December 2010

Keywords:
ERN
Theta
DTI
Diffusion imaging
Connectivity
Oscillation
Synchrony
EEG

ABSTRACT

Studies on electrophysiological signatures of error processing have focused on the medial frontal cortex, although widespread neuroanatomical networks support error/action monitoring. Here, electrophysiological responses to errors were combined with structural white matter diffusion tensor imaging (DTI) to investigate the long-range anatomical networks that support error processing. The approach taken here was to link individual differences in error-related EEG responses to individual differences in white matter connectional anatomy. Twenty subjects performed a speeded instructed choice task (a variant of the Simon task) designed to elicit response errors, and also underwent DTI scanning in a separate session. In the EEG data, significantly enhanced theta (4–8 Hz) oscillations were observed over medial frontal electrodes (centered on FCz) during response errors. Mid-frontal scalp sites (likely reflecting medial frontal cortex activity) also functioned as a strong "hub" for information flow, measured through theta-band phase synchronization degree. Next, a dipole source of the error-related theta-band activity was localized for each subject, accounting for approximately 80% of the topographical variance. Correlating individual differences in medial frontal theta dynamics with white matter tracts linking these dipole sources to the rest of the brain revealed that subjects with stronger error-related theta also had stronger white matter connectivity with the ventral striatum and inferior frontal gyrus. Further, subjects in whom medial frontal regions acted as a stronger synchronization "hub" had stronger connectivity between the dipole source location and the corpus callosum and dorsomedial prefrontal white matter pathways. These findings provide novel evidence for the role of widespread fronto-striatal networks in monitoring actions and signaling behavioral errors.

Introduction

Impairments of action monitoring are implicated in a wide range of brain disorders (Olvet and Hajcak, 2008) from substance abuse (Potts et al., 2006) to schizophrenia (Bates et al., 2009; Morris et al., 2006) to autism spectrum disorders (Vlamings et al., 2008). Within healthy populations, individual differences in action monitoring have been linked to political preferences and personality styles (Amodio et al., 2007; Larson et al., 2010). Clearly, a better understanding of the neural networks that support action monitoring and error processing is relevant for basic psychological and neuroscience theories as well as for understanding cognitive control impairments in patient groups.

Investigations into neurophysiological responses to errors have largely focused on the "error-related negativity," which refers to a relatively negative polarity in the time-domain averaged EEG waveform immediately following response errors (Falkenstein et al., 2000; Gehring et al., 1993; van Veen and Carter, 2002). However, although over 400 articles can be found on PubMed when searching "error negativity," much remains unknown about the neural mechanisms that generate this negativity. Physiologically, these error-related electrical dynamics might reflect coordinated theta-band (4–8 Hz) oscillations (Luu and Tucker, 2001; Trujillo and Allen, 2007). Theta is a prominent frequency band observed in direct recordings of the medial prefrontal cortex in humans (Cohen et al., 2008b; Wang et al., 2005) and nonhuman primates (Tsujimoto et al., 2006; Tsujimoto et al., 2010; Womelsdorf et al., 2010). At the cognitive level, medial frontal theta has been linked to error monitoring and feedback processing during learning tasks (Bates et al., 2009; Cavanagh et al., 2009; Cohen et al., 2008b; Holroyd and Coles, 2002; Mazaheri et al., 2009; Trujillo and Allen, 2007; Wang et al., 2005). At the neurobiological level, theta has been implicated in synaptic mechanisms of learning, information coding, and inter-regional communication (Dragoi and Buzsaki, 2006; Huerta and Lisman, 1995; Jensen and Lisman, 2000), in part by regulating spike timing and providing temporal windows to allow co-activation of spatially disparate but functionally connected networks of neurons. Thus, medial frontal theta is a neurobiologically plausible mechanism by which this region may coordinate local and long-range neural networks to monitor actions and detect response errors.

* Department of Psychology, University of Amsterdam, Roetersstraat 15, 1018 WB, Amsterdam, The Netherlands.
E-mail address: mikexcohen@gmail.com.

1053-8119 © 2010 Elsevier Inc. Open access under the Elsevier OA license.
doi:10.1016/j.neuroimage.2010.12.072

Consistent with the idea that theta-band oscillations support long-range functional connectivity with the medial frontal cortex, theta-band synchronization between the medial and lateral frontal electrodes (Cavanagh et al., 2009) and estimated cortical locations (Hanslmayr et al., 2008), between medial frontal cortex and nucleus accumbens (Cohen et al., 2009b), and between medial frontal and occipital cortices (Cohen et al., 2009d), have been linked to error processing and reward learning. These findings suggest that distributed networks underlie neural responses to errors. Indeed, the amplitude of the error-related negativity is attenuated in patients with lesions to medial prefrontal cortex (Cohen et al., 2008b; Stemmer et al., 2004; Swick and Turken, 2002), lateral prefrontal cortex (Gehring and Knight, 2000; Ullsperger et al., 2002), and basal ganglia nuclei (Ullsperger and von Cramon, 2006). Even when gray matter is intact but the white matter behind the prefrontal cortex is lesioned, the error-related negativity is attenuated (Hogan et al., 2006). This latter finding demonstrates the importance of long-range white matter connectivity in generating error-related medial frontal responses, and is consistent with correlations between local white matter and the time-domain averaged error-related negativity (Danielmeier et al., 2010; Westlye et al., 2009). More generally, these findings support the idea that the medial frontal cortex is a fulcrum for cognitive control processes, and can interact with multiple brain systems involved in sensory, motor, emotional, and social processing, to adapt behavior flexibly according to goals or internal/external feedback.

Here structural correlates of medial frontal error-related theta dynamics were examined. Twenty subjects performed a speeded response-time task in which response errors occurred often. Error-related theta cortical responses were source-estimated, and structural white-matter connectivity from this dipole location was examined. Further, white matter connectivity was correlated with the extent to which medial frontal sites were an information "hub" for long-range cortico-cortical phase synchronization (functional connectivity). Whereas error-related theta power at medial frontal sites predicted white matter connectivity between the estimated source (usually in the anterior cingulate) and motor, ventral striatal, and right ventrolateral prefrontal regions, medial frontal functional connectivity predicted white matter connectivity between the estimated source and fibers in the corpus callosum and dorsomedial prefrontal cortex. This multi-method, cross-subjects approach illustrates how anatomical and functional networks contribute to medial frontal error-related electrophysiological dynamics.

Methods

Participants

Twenty subjects (10 male; average [stdev] age 22 [2.5]) volunteered in exchange for course credit or money (€48). Subjects had normal or corrected-to-normal vision and no reported history of psychosis, brain disease or psychiatric illness, or significant drug usage. The local ethics committee at the University of Amsterdam approved the experiment, and subjects provided informed consent prior to the start of the experiment. Data were collected over three sessions, one MRI session and two EEG sessions.

Task

The task was an auditory–visual Simon task. On each trial a visual (small gray box) and auditory (sine-wave tone) stimulus were presented either on the right or left visual/auditory hemifield. Auditory stimulation was delivered through plastic EEG-compatible earphones that subjects plugged into each ear. Subjects were instructed to respond with the left or right hand according to the presentation side of the auditory or visual stimulus. Every 10 trials, a screen appeared that instructed subjects to respond to the visual or auditory domain. The stimuli were presented for 50 ms, followed by an 1150 ms window in which subjects could respond. The inter-trial-interval varied between 1000 and 1500 s. No performance feedback was provided. Auditory and visual stimulus presentation sides were pseudo-randomized such that there was an equal number of subsequent trial pairings: previous trial congruent, current trial congruent; previous trial incongruent, current trial congruent; and so on. In the present set of analyses, only congruent–congruent and error trials were examined. There were 2400 trials over two sessions. Subjects first received instructions and one training block before the experiment began.

EEG acquisition and processing

EEG data were acquired at 512 Hz from 64 channels placed according to the international 10–20 system, from peri-occular and electromyographic electrodes on the thumbs, and from both earlobes (used as reference). Offline, EEG data were high-pass filtered at 0.5 Hz and then epoched from −1.5 to +2.5 s surrounding each trial (to avoid edge artifacts resulting from wavelet filtering). All trials were visually inspected and those containing EMG or other artifacts not related to blinks were manually removed. Independent components analysis was computed using eeglab (Delorme and Makeig, 2004) software, and components containing blink/oculomotor artifacts or other artifacts that could be clearly distinguished from brain-driven EEG signals were subtracted from the data. This was done separately for each testing session, because minor differences in cap placement or other state variables may affect component estimation with respect to blinks/oculomotor artifacts. Finally, data were separately analyzed both before and after current-source-density transform (Kayser and Tenke, 2006). Current-source-density (CSD) is a spatial filter that increases topographical selectivity by effectively subtracting out spatially broad and therefore likely volume-conducted effects. This approach has been validated for investigating inter-electrode synchronization (Srinivasan et al., 2007; Winter et al., 2007). The units of the data after this transform are $\mu V/cm^2$. The unfiltered "voltage" data (μV) were used for dipole source modeling.

EEG analyses

Time–frequency decomposition was done as in our previous studies (e.g., Cavanagh et al., 2009; Cohen et al., 2009b). Briefly, a wavelet decomposition analysis was performed in which all trials from one channel were concatenated in time, the power spectrum of which (obtained from the fast-Fourier-transform) was multiplied by the power spectrum of a complex Morlet wavelet ($e^{i2\pi tf}e^{-t^2/(2*\sigma 2)}$, where t is time, f is frequency, which increased from 1 to 30 Hz in 25 logarithmically spaced steps, and σ defines the width of each frequency band, and is set according to $4/(2\pi f)$), and the inverse fast-Fourier-transform was taken. This is equivalent to but more efficient than single-trial convolution. This procedure was done separately for each channel and condition. From the resulting complex signal from each convolution, an estimate of frequency-band specific power at each time point is defined as the squared magnitude of the result of the convolution $Z\,(\mathrm{real}[z(t)]^2+\mathrm{imag}[z(t)]^2)$, and an estimate of frequency-band specific phase at each time point is the angle of the convolution result. Relatively long epochs were cut from the continuous EEG data because of edge artifacts due to sudden transitions in signal values between trials. Visual inspection confirmed that edge artifacts subsided well before the time windows used in analyses (−1000 to +1000 ms surrounding each response). Taking long epochs and trimming edge artifacts is preferred over Hanning or other windows, because the latter method will attenuate real signal, while the former method does not. Power was normalized using a decibel (dB) transform (dB power = 10*log10 [power/baseline]), where the baseline activity was taken as the average power at each frequency band, averaged across conditions, from −300 to −100 ms pre-stimulus. DB conversion ensures that all frequencies, time points, electrodes, conditions, and subjects are in the same scale

and thus comparable. The precise time window for baselining would not impact the error-correct differences, however, because the baseline is constant across conditions.

Frequency band-specific phase synchronization (functional connectivity) was computed according to $\left|\frac{1}{n} * \sum_{t=1}^{n} e^{i[\phi_{jt}-\phi_{kt}]}\right|$, where n is the number of trials, and φ_j and φ_k are the phase angles of electrodes j and k. This is an index at each time–frequency point of the consistency of phase angle differences between two electrodes over trials. This was computed between each pair of electrodes. Subsequently, average synchronization from 4–8 Hz and −50 to +150 ms surrounding the time of button press was taken into an analysis of network activity based on principles of graph theory. Graph theory provides a mathematical framework with which to conceptualize and quantify local and global network characteristics. Applied to EEG, each electrode (and the underlying tissue from which it measures) may be considered a node, and each possible connection between pairs of electrodes may be considered a vertex. Each node could have a maximum of 63 vertices (connections to all electrodes minus itself). However, only vertices that are robust (i.e., reflecting strong functional connectivity) should be considered. Thus, a threshold is applied (described below), and each electrode can be assigned a value–termed synchronization degree–according to the number of supra-threshold vertices it has (i.e., the number of electrodes with which there is robust functional connectivity). Electrodes with relatively large synchronization degree may be considered a "hub" or "intersection" for information flow. Synchronization degree can be computed separately for each frequency band, window of time, electrode, and condition. The threshold was set to one standard deviation above the median of each subject's inter-regional phase synchronization distribution, thus producing a subject-specific data-based thresholding approach. Preliminary testing demonstrated that different thresholds had minimal effect on the overall topographical distributions and condition differences (data not shown). Differences in degree across condition were tested with paired sample t-tests. All statistical tests based on parametric statistics approximated normal distributions, as evidenced by a failure to disconfirm the null hypothesis of normally distributed data (Shapiro–Wilk test, p-values>0.12).

Dipole source modeling

Dipole source modeling was implemented in eeglab (Delorme and Makeig, 2004) using the function dipfit_erpeeg with default parameters. A standard boundary-element-model was used for localization. Subject-specific head models based on T1 images were not used because precise electrode positions were not available. For each subject, the average theta power difference between correct and error trials from −50 to +150 ms at each electrode was entered into the dipole estimation. Note that the purpose of this analysis was not to identify a putative single generator of cortical error-related theta; rather, the purpose was to obtain a subject-specific and data-driven seed region for the DTI tractography analyses (see next section). Thus, one dipole was estimated per subject. Preliminary testing indicated that fitting two dipoles per subject provided little improvement on the residual variance (~1–5% improvement), and usually resulted in bilateral dipoles in similar locations as the single dipole source. Using only one dipole also has the advantage of being more suitable for fiber tracking analyses. Data from one subject were removed from this analysis because the dipole was located outside the brain. In a few cases, the dipole sphere included voxels that were located inside the ventricle in diffusion-image space. Visual inspection confirmed that tracts still looked reasonable from the entire seed mask, and so the masks were not altered.

A second set of dipoles was estimated based on independent components. For each subject, an independent components analysis was conducted on correct and error trials aggregated over the two sessions, and the component with a broad medial frontal focus was selected. A dipole source of this component was estimated (using the eeglab function dipfit and a boundary-element-model); the rest of the statistical procedures for computing tractography and correlating with EEG dynamics (detailed below) was the same as for the dipole based on the observed theta response. The purpose of this alternative procedure for estimating a dipole used as a seed region for white matter fiber tracking was to ensure that the results reflected stable and robust individual differences in structure and function both when using the observed data (theta power) and when using an electrode weighting based on isolating a temporally independent medial frontal dynamic (independent component). For convenience, analyses using the medial frontal component or tractography based on those dipoles are referenced with "IC" (e.g., IC-seeded tractography). Data from one subject were removed from this analysis because the dipole was in the cerebellum.

Diffusion-tensor imaging (DTI) data

DTI data were acquired on a 3 T Phillips MRI scanner at the Amsterdam Medical Center of the University of Amsterdam. Parameters were as follows: TR 9.1948, TE 65, 60 2-mm thick slices, matrix size 128×128, and in-plane resolution 2×2 mm^2. For diffusion directions, 50 equidistant points along a unit sphere were created. Images with no diffusion were also acquired. Four repetitions of this scan sequence were acquired to maximize signal-to-noise ratio. In total, DTI scanning lasted about 45 min. In the same session, a high-resolution T1 scan was also acquired. Preprocessing of DTI data was done according to standard protocols in FSL software, primarily bedpostX (Behrens et al., 2007) (www.fmrib.ox.ac.uk/fsl).

Linking DTI and EEG data

Probabilistic tractography was computed from a 5-mm Gaussian sphere surrounding the dipole coordinate for each subject. A Gaussian sphere instead of a single point has the advantage of providing a slightly less spatially restrictive seed and thus accounts for some spatial uncertainty, e.g., due to using standard electrode positions. The result of the tractography analysis is a brain volume of probability values that correspond to the number of pathways starting in the seed region and passing through that voxel. Five thousand paths from each voxel in the seed region were generated. The resulting "tract strength" volume was used in a voxel-based analysis, in which tract strength was correlated, across subjects, with brain or behavior indices (FCz theta power, FCz synchronization degree, task error rate, and post-error slowing), using Spearman's rank-order correlation (tract strength values are non-normally distributed so nonparametric correlations are appropriate). See Fig. 5 for a graphical overview of the analysis. Because tractography is probabilistic, some of the weakest paths may be noise; therefore it is common practice to remove the weaker paths across subjects (e.g., Aron et al., 2007). Here, only voxels with group-average tract strengths greater than 100 were used, which corresponds approximately to removing the weakest 5% of tracts across subjects. This resulted in testing 66,576 voxels (29.14% of brain voxels). For statistical thresholding, a p-value of 0.005 and a contiguous cluster threshold of 15 voxels (120 mm^3) were used. This cluster threshold was relaxed for the IC-dipole analysis because the clusters were smaller, though in similar locations as the theta-dipole analysis. Significant correlation clusters were then projected back onto an MRI and displayed using fslview (MRI viewing program in the FSL package). This conjoint voxel- and cluster-level threshold helps protect against false positives. These analyses were conducted in Matlab.

Results

Behavioral results

Errors were made on 7.1% of trials (average of 170 error trials per subject; standard deviation 4.1%). Reaction times were 382 ms

(standard deviation 15 ms) for error and 401 ms (14 ms) for correct trials, a significant difference ($t_{19}=3.27$, $p=0.004$).

Response errors elicit medial frontal theta activity

As seen in Fig. 1A, response-related activity elicited increased theta power in medial frontal sites centered on FCz during both correct ($t_{19}=5.17$, $p<.001$) and error ($t_{19}=11.15$, $p<.001$) trials. Repeated-measures ANOVA demonstrated that error trials elicited significantly more theta power compared to correct trials ($F_{1,19}=102.17$). CSD maps (Fig. 1B) confirm that this medial frontal error-related theta response was localized selectively to medial frontal scalp regions. As with non-spatially filtered data, CSD transformed FCz power was greater than pre-trial baseline during correct ($t_{19}=10.84$) and error ($t_{19}=9.56$) trials, and was greater during error compared to correct trials ($F_{1,19}=75.95$). Time–frequency power plots from FCz demonstrate the temporal-frequency specificity of this effect (Figs. 2A–B). Time–frequency decomposition of the IC for each subject (which was selected based on topographical characteristics and not on the basis of condition differences or frequency characteristics; see Fig. 1C) showed a similar pattern of time–frequency characteristics as the data recorded at FCz (Fig. 2C), which justifies its use in the DTI tractography analyses.

The medial frontal cortex may be a "hub" for theta-band functional connectivity

When examining inter-regional synchronization among electrodes, each electrode may be conceptualized as a "hub" for information flow. Graph theory provides an analytic approach to quantifying "hubness" of each node (electrode), here defined as the number of other electrodes with which each electrode is strongly phase synchronized (see Methods); higher numbers (i.e., greater degree) indicate that that electrode is relatively more richly functionally connected to other cortical areas.

Consistent with a role of medial frontal theta in coordinating widespread cortical networks during cognitive control, theta synchronization degree was most robust over FCz and surrounding electrodes (Fig. 3, top row), and was significantly stronger during errors compared to correct responses ($F_{1,19}=12.26$, $p=.002$). In contrast, no topographically robust hubs were observed in alpha; beta/low gamma (20–30 Hz) demonstrated robust hubs in anterior and lateral prefrontal regions, but this was not significantly related to errors (Fig. 3, bottom row). Note that this connectivity analysis is not possible with the IC data because a single component represents a weighted sum of all electrodes whereas this connectivity analysis treats each electrode as independent.

To examine the relationship between inter-regional long-range phase synchronization and local theta dynamics, theta power was correlated with theta synchronization degree at each electrode. Significant correlations were observed only in medial and lateral frontal regions (Fig. 4) (p-values for FCz, C4, and C5 all less than 0.001). There were strong power-synchrony degree correlations at lateral sites, although there was little increase in oscillation power in these regions (Fig. 4). Finally, beta-band (20–30 Hz) power and phase synchronization degree were not significantly correlated at anterior frontal sites in which synchronization degree was robust (all p-values greater than 0.2). In other words, medial frontal theta power and synchronization degree significantly correlated, whereas power and synchronization were decoupled in other regions and frequency bands. As outlined further in the Discussion, these observations provide counterevidence for a simple alternative explanation that phase synchronization is driven by power fluctuations. Instead, these results suggest that theta-band activity recorded over medial frontal cortex reflects a neurocognitive mechanism for coordinating both local and long-range neural networks that support cognitive control.

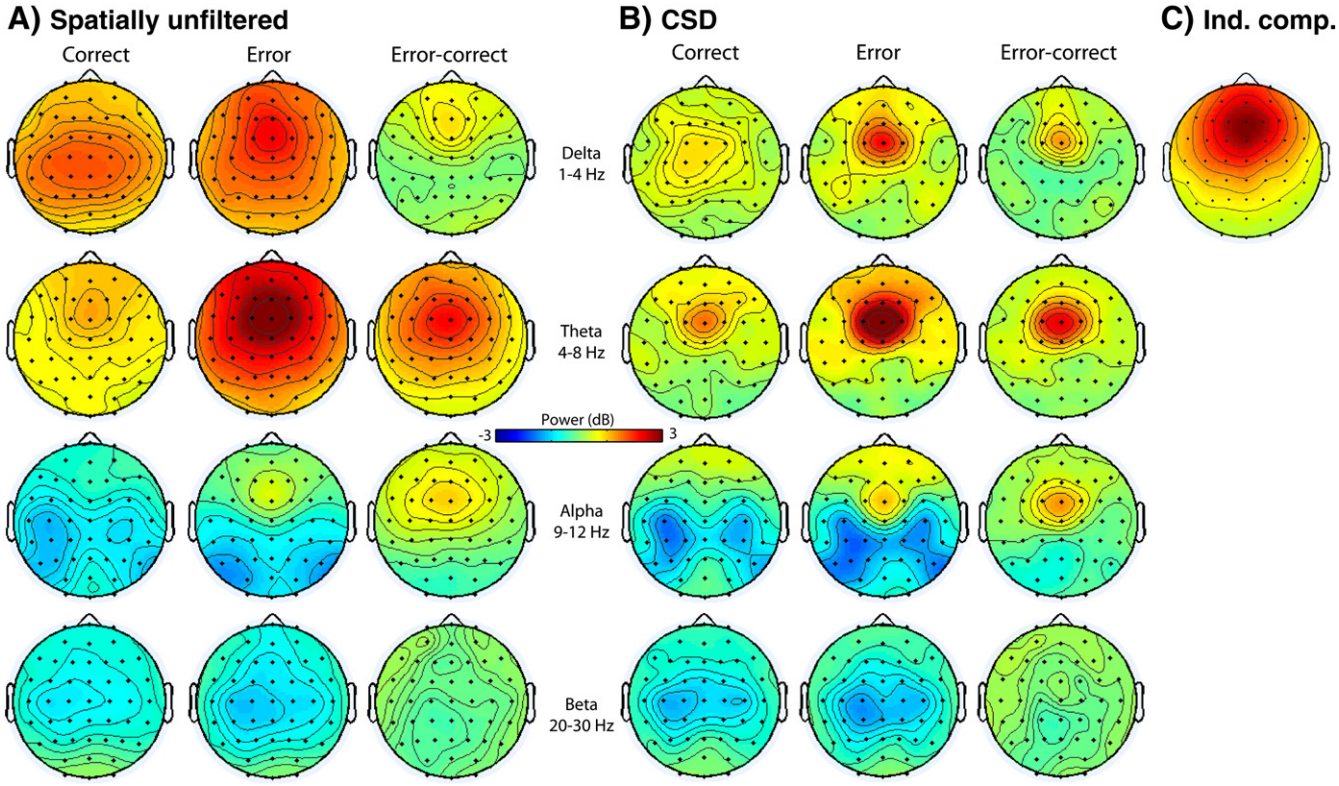

Fig. 1. Topographical distributions of task-related frequency band-specific oscillation power for (A) spatially unfiltered and (B) current-source-density (CSD) filtered data, averaged from −50 to +150 ms surrounding the response. Rows contain different frequency bands; columns, conditions and condition differences. Panel (C) shows the average topographical projection of the independent component selected for each subject.

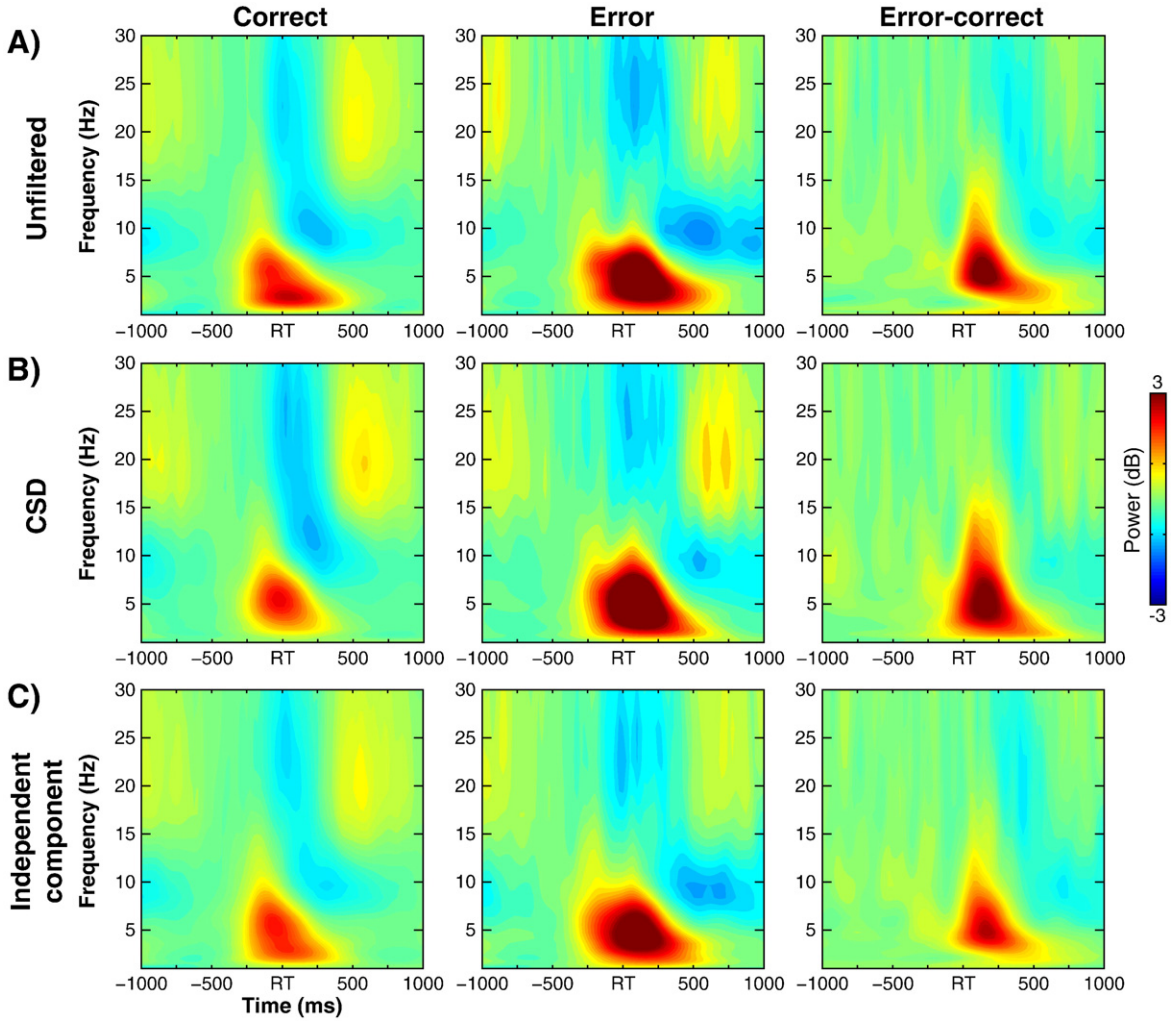

Fig. 2. Time–frequency plots of oscillation power as a function of condition and condition differences, from electrode FCz. Top row shows power from spatially unfiltered data; middle row shows power from CSD transformed data; bottom row shows power from the independent component, which was selected on the basis of topographical distribution (see Fig. 1C). Note that CSD spatial filtering preserves local activity while enhancing spatial resolution (c.f. Figs. 1A–B).

Error-related medial frontal theta oscillations and functional connectivity predict distinct white matter anatomical networks

In this set of analyses, individual differences in cortical electrophysiological activity were correlated with individual differences in white matter connectivity; the goal was to gain insight into the anatomical networks underlying error-related medial frontal theta activity. Details of this analysis are in the Methods, but briefly: A dipole source of the error-correct theta topographical map was estimated for each subject, and this dipole was used as a seed region for probabilistic tractography from that subject. Subsequently, "tract strength" values were correlated with physiological measures (FCz power and inter-regional synchronization degree) across subjects; regions in which at least 15 contiguous voxels that are each significant at $p<0.005$ were considered significant (see Fig. 5). Thus, measures of subject-specific brain anatomy were correlated with measures of subject-specific brain electrophysiology. All significant clusters are listed in Table 1.

Most dipoles were located in the anterior cingulate cortex or surrounding tissue (Fig. 6). Each subject's single dipole accounted for 81.88% (10.18% stdev) of his or her unique error-related theta topography. The IC-dipole accounted for 96.37% (2.4% stdev) of the IC weight topography. This difference in explained variance is not surprising, considering that the theta-dipole modeled the observed data whereas the IC-dipole modeled a temporally isolated component of the data. Dipole depth (Z-coordinate) did not significantly correlate with FCz error-related theta power ($r=0.20$, $p=0.39$), which provides evidence against a potential confound that larger scalp potentials lead to deeper sources, which would in turn drive differences in anatomical networks across subjects.

Subjects with stronger error-related medial frontal (FCz) theta power had stronger white matter connectivity between the dipole seed regions and the ventral striatum, motor cortex, and areas of the ventrolateral prefrontal cortex (Fig. 7A). No significant negative correlations were observed. Results from the IC-seeded tractography analysis yielded similar results in the motor areas and inferior frontal cortex (Fig. 7B), although there was no significant correlation in the ventral striatum.

In contrast, subjects in whom FCz was a relatively stronger "hub" for theta-band functional connectivity had stronger white matter connectivity from the dipole seed region through the corpus callosum and white matter behind the superior frontal gyrus (Fig. 8A). No significant negative correlations were observed. IC-seeded tract strength correlated with FCz synchronization degree in bilateral middle frontal white matter tracts (Fig. 8B). Within the corpus callosum voxels identified in the theta-seeded tractography strength, IC-seeded tractography strength also correlated with FCz synchronization degree ($r=.50$, $p=.023$).

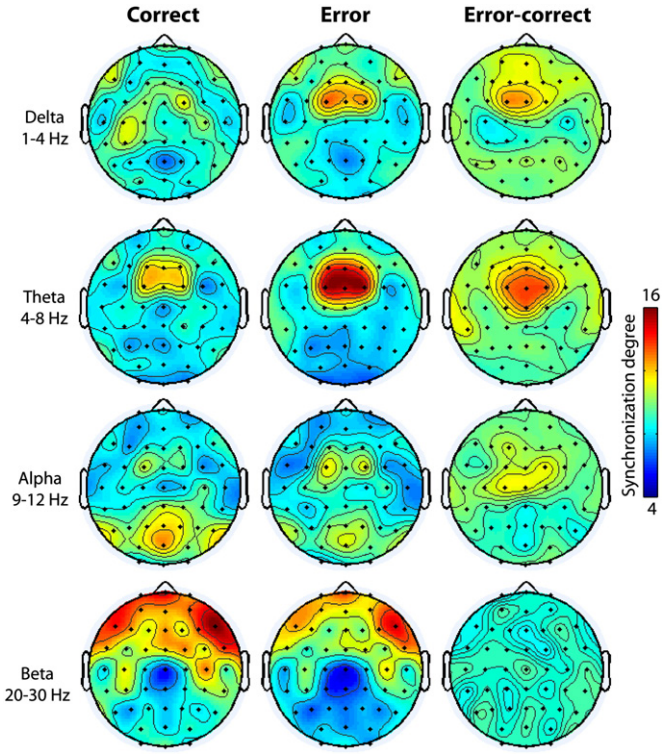

Fig. 3. Topographical distributions of frequency band-specific synchronization degree, plotted by condition and condition differences. "Hotter" colors indicate a greater number of long-range cortico-cortical functional connections (phase synchronization) centered on each electrode position.

Differences between the size of the correlation coefficients between tract strength and FCz theta, and tract strength and synchronization degree, were also tested; this analysis would support statistically robustly dissociable networks underlying theta power and theta inter-regional synchronization. Results for each region are listed in Table 1. Most correlations were not statistically significantly different, except the corpus callosum, which showed modestly stronger correlation with synchronization degree compared to power ($p = .027$, which would not survive correction for multiple comparison across 6 regions).

Error-related theta source dipole-seeded white matter tracts were also correlated with two different task performance indices: overall error rate and post-error slowing. No clusters exceeded the significance threshold in either analysis, even with a more liberal statistical threshold of $p = .01$.

Discussion

Here it was shown that cortical electrophysiological responses to performance errors comprise an increase in medial frontal oscillation power and medial frontal theta-band long-range phase synchronization with other cortical areas. Individual differences in these medial frontal theta dynamics correlated with individual differences in anatomical white matter pathways connecting the putative dipole source of the medial frontal theta to the ventral striatum, motor cortex, and lateral/anterior prefrontal regions.

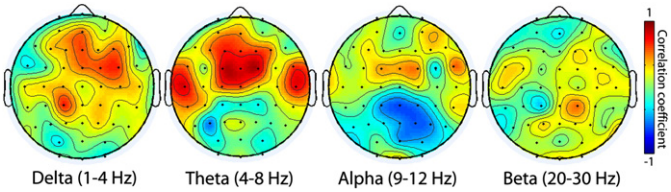

Fig. 4. Topographical map of correlation coefficients between frequency band-specific phase synchronization degree and power at each electrode.

The precise function of the medial frontal cortex remains debated, although it clearly is involved in action monitoring and flexible adaptation of behavior (Ridderinkhof et al., 2004). Prominent thinking suggests that the medial frontal cortex signals the error and recruits lateral regions to implement adjustments (Egner and Hirsch, 2005b; Kerns et al., 2004). Medial frontal cortex may additionally provide top-down control signals to influence processing in sensory and/or motor systems (Cohen et al., 2009d; Egner and Hirsch, 2005a; King et al., 2010; Rushworth et al., 2007). The present findings suggest that the medial frontal cortex may use synchronized neurophysiological theta oscillations to functionally interact with other cortical and subcortical areas. Further, these interactions may be shaped by the strength of white matter pathways.

Medial frontal theta dynamics and cognitive control

Medial frontal theta is widely observed during situations involving action monitoring, cognitive control, and reinforcement learning (Cavanagh et al., 2009; Christie and Tata, 2009; Cohen et al., 2007; Marco-Pallares et al., 2008; Trujillo and Allen, 2007). Sustained medial frontal theta is also observed during working memory delays (Khader et al., 2010; Onton et al., 2005), and other memory functions (Sauseng et al., 2010). Thus, an interesting avenue of study would be to examine whether there is a common neurocognitive process underlying these seemingly disparate functions, or whether medial frontal theta is a general neural organization scheme that can be used to support many different processes subserved or orchestrated by the medial frontal cortex. Indeed, the observation of FCz as a strong "hub" for functional connectivity in the theta range is consistent with the latter idea. Regardless, medial frontal theta provides a window into a neurobiologically plausible mechanism for information processing and transfer, and therefore is a useful index for investigating the mechanisms by which prefrontal cortex may engage control mechanisms.

In terms of the generator of this medial frontal theta activity, pre-supplementary motor area or anterior cingulate cortex is a likely candidate, considering the convergent findings from direct recordings in humans (Cohen et al., 2008b; Wang et al., 2005), other dipole studies of EEG and MEG data (Debener et al., 2005; Miltner et al., 2003; Vocat et al., 2008), and functional MRI studies (Mathalon et al., 2003; van Veen and Carter, 2002). One may question the physiological plausibility of a single dipole to explain an entire cortical topography; it is possible that more distributed sources contribute to the topography. Considering that this dipole reflected ~82% of the single-subject theta topography, it seems likely that the region identified by the dipole analysis contributes to but does not explain each subject's cortical error processing. As mentioned in the Methods, the purpose of this dipole analyses was not to localize a putative single origin of the observed topography, but rather to identify a data-driven appropriate seed region for tractography to link brain structure to function.

In addition to coordinating local activity, as measured by increased FCz power, theta oscillations seem to have a role in coordinating long-range functional connectivity during cognitive control. This follows up on our previous work, in which we found error-related enhanced synchrony between FCz and lateral frontal (Cavanagh et al., 2009) and occipital (Cohen et al., 2009d) electrodes. Here an alternative approach was taken that focuses more on the topographical distribution of "hubs" rather than the specific cortical targets of synchronization. Graph theory-based analyses are increasingly used to characterize spatially broad networks in normal cognitive processes (Palva et al., 2010) and brain diseases such as schizophrenia and Alzheimer's (Micheloyannis et al., 2006; Stam et al., 2007). The present findings strongly implicate the medial frontal cortex as the

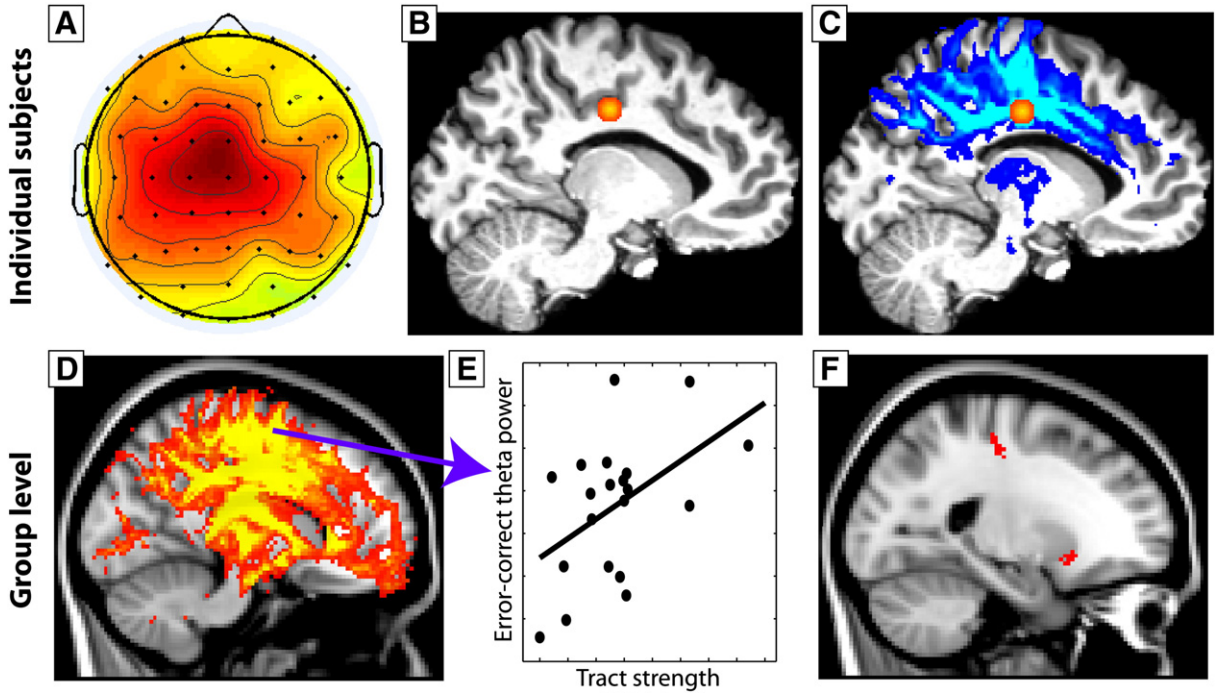

Fig. 5. Graphical overview of analysis procedure for linking cortical electrophysiology to individual differences in white matter connectivity. Top row shows procedure applied to each subject; bottom row shows group-level procedure. Each subject's topographical response-locked error-correct theta power distribution (A) was used for dipole estimation (B), which was used as a seed (the dipole voxel and a surrounding Gaussian sphere) for probabilistic tractography (C). At each voxel that had strong connectivity across subjects (D), individual differences in tract strength were correlated with the error-correct theta power difference at electrode FCz (E; each dot represents a subject). Finally, tract strength maps were thresholded such that only clusters of statistically robust correlations were displayed (F).

fulcrum of a neural network involved in monitoring behavior for errors. Further, the findings presented in Fig. 3 suggest that this error-related cortical network is also specific to the theta-band, because, for example, strong synchrony hubs in the anterior–lateral prefrontal cortex in the beta band were not modulated by whether the response was correct or an error.

A simple alternative explanation to phase synchrony results is that they co-occur with increased power (or increased signal-to-noise-ratio). Although with large power, phase values are better estimated (at the other extreme, with zero power it is not possible to estimate phase), power and phase are mathematically independent (except when power is very close to zero, which in practice is not often observed at neurocognitively relevant frequencies in EEG data). Nonetheless, this is a potential concern in the present study because both theta-band power and theta-band phase synchronization increased around electrode FCz. However, the present findings provide counterevidence for this simple alternative explanation. Specifically, the observations that (1) power and phase synchrony correlate selectively in some frequency bands and at some electrodes, and (2) such correlations are observed even when no robust task-related changes in power occurred (e.g., theta at lateral prefrontal sites) cannot be explained by the power-drives-synchrony argument. Thus, it appears that power and inter-site phase synchronization reflect different but related mechanisms to coordinate local and long-range neural networks.

White matter connectivity networks supporting error processing

Cross-subject correlations between error-related FCz theta power and dipole seeded tractography suggest a broad fronto-striatal network contributing to error-related medial frontal electrophysiological dynamics.

Table 1
List of significant correlations between error-related theta dipole source tractography and EEG dynamics.

Region	XYZ (MNI)	Cluster size (mm^3)	r_p (p-value)	r_s (p-value)	r_p–r_s p-value
Theta-dipole					
Ventral striatum	−26 10 −8	56	.70 (.001)	.310 (.195)	.062
Ventrolateral PFC	−44 34 −2	44	.647 (.002)	.515 (.023)	.285
Motor	−22 −22 48	82	.714 (<.001)	.496 (.032)	.160
Superior frontal gyrus	−18 34 32	36	.722 (<.001)	.680 (.001)	.407
Superior frontal sulcus	−22 24 28	98	.478 (.038)	.608 (.005)	.300
Corpus callosum	6 0 24	482	.265 (.272)	.738 (<.001)	.027
IC-dipole					
Ventrolateral PFC	−28 54 −4	14	.679 (<.001)	.411 (.071)	.127
Motor	−28 −20 64	24	.703 (.0005)	.471 (.036)	.145
Left middle frontal gyrus	−32 2 52	13	.494 (.026)	.664 (.001)	.226
Right middle frontal gyrus	32 8 48	11	.568 (.009)	.792 (<.001)	.103

Notes. XYZ are 3D coordinates in Montreal Neurological Institute standard space of the maximum correlation voxel within each cluster. Cluster size is reported in mm^3. r_p = correlation coefficient for tract strength-FCz power analysis; r_s = correlation coefficient for tract strength-synchronization degree analysis; r_p–r_s p-value is the significance value testing whether the correlation coefficients for the two analyses are significantly different. All correlations are tested using the average tract strength value from all voxels within each mask. P<.005 is the map-wise significance threshold, with 15 contiguously significant clusters (this constraint was relaxed for the IC-dipole analysis).

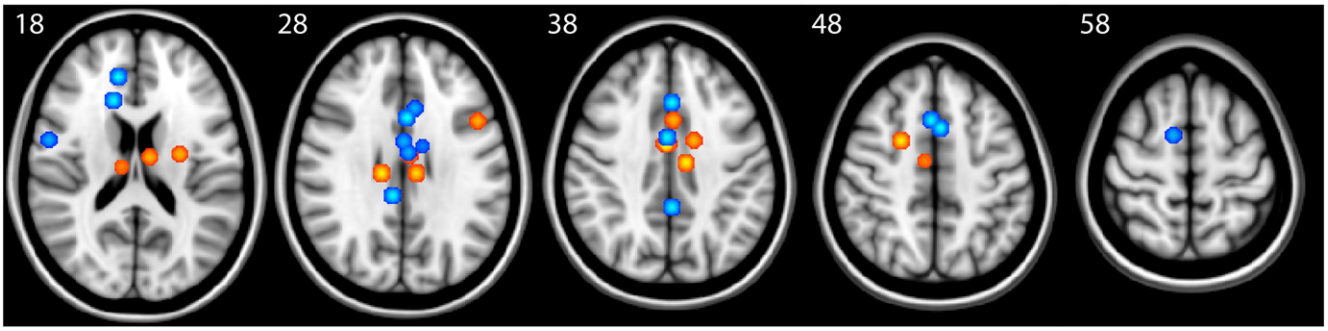

Fig. 6. Dipole locations of error-correct theta activity for some subjects. Red shows dipoles of the theta error-correct activity; blue shows dipoles of the independent components. White numbers indicate MNI Z-coordinate.

The correlation in the striatum is particularly interesting given the monosynaptic anatomical connectivity from regions of the medial frontal cortex to the ventral striatum (Haber et al., 1995). Simultaneous recordings of surface EEG and nucleus accumbens EEG in deep-brain-stimulation patients repeatedly demonstrate functional electrophysiological links between the medial frontal cortex and ventral striatum during cognitive control (Münte et al., 2007) and reward tasks (Cohen et al., 2009a, 2009b). These findings are consistent with computational models that implicate striatal functioning in error-related medial frontal activity (Holroyd and Coles, 2002). Although it is not possible to determine directionality in DTI data, histological tracing (Haber et al., 1995) and electrophysiological "directed" synchrony measures (Kasanetz et al., 2006; Montaron et al., 1996) suggest that medial frontal cortex may provide a direct "top-down" signal to the striatum (Cohen et al., in press). The voxels in the ventral striatal region identified in this analysis are also close to a region near the medial insula in which fractional anisotropy correlates with awareness of response errors (Danielmeier et al., 2010). The correlations in white matter near the inferior frontal cortex are consistent with the role of lateral prefrontal regions in cognitive control processes (Forstmann et al., 2008). Indeed, findings from patients with lesion to the lateral prefrontal cortex confirm this region's involvement in generating medial frontal error-related potentials (Gehring and Knight, 2000). The consistency of the striatal and frontal correlations with previous empirical findings also helps validate the approach of combining EEG and DTI using cross-subject correlations.

In contrast to the correlations with theta power, theta-band synchronization degree predicted individual differences in tract strength in the corpus callosum and fibers leading to the superior frontal gyrus. This is indeed a sensible result considering that synchronization degree measures the extent to which medial frontal cortex is a "hub" or intersection for long-range cortico-cortical functional connectivity. Demonstrating that long-range cortico-cortical functional connectivity correlates with corpus callosum pathways further helps establish the validity of the approach of linking DTI and EEG to understand brain functional architecture. Indeed, this finding is consistent with recent reports linking visual stimulus-evoked gamma oscillations to corpus callosum integrity (Zaehle and Herrmann, 2011), and also resting-state EEG connectivity (Teipel et al., 2009). Because this analysis was based on synchronization degree difference between error and correct trials, this result does not simply reflect stable trait differences in connectivity, but rather specific increases in functional coupling resulting from errors.

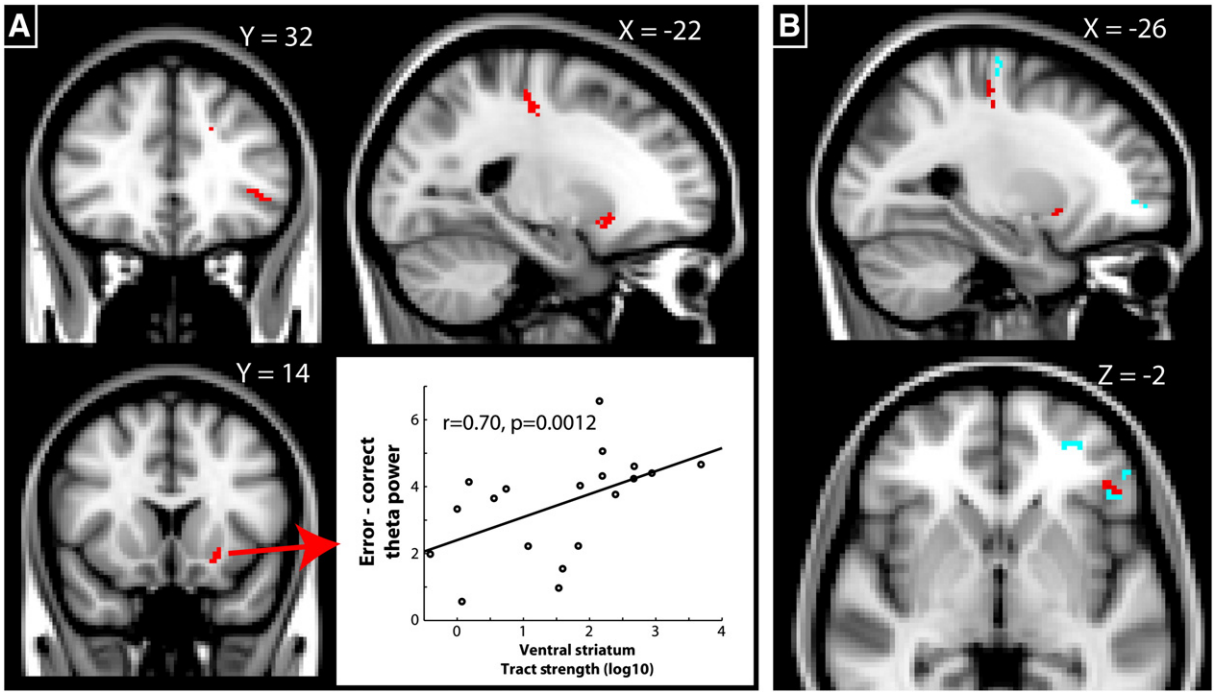

Fig. 7. Subjects with larger error-related medial frontal theta power had stronger white matter tracks linking the error-theta dipole source (A) to white matter surrounding the ventral striatum, motor cortex, and inferior frontal cortex. As an example of this correlation, the scatter plot shows the relationship across subjects for the voxels in the ventral striatum. Panel (B) shows the results from the IC-dipole (in blue).

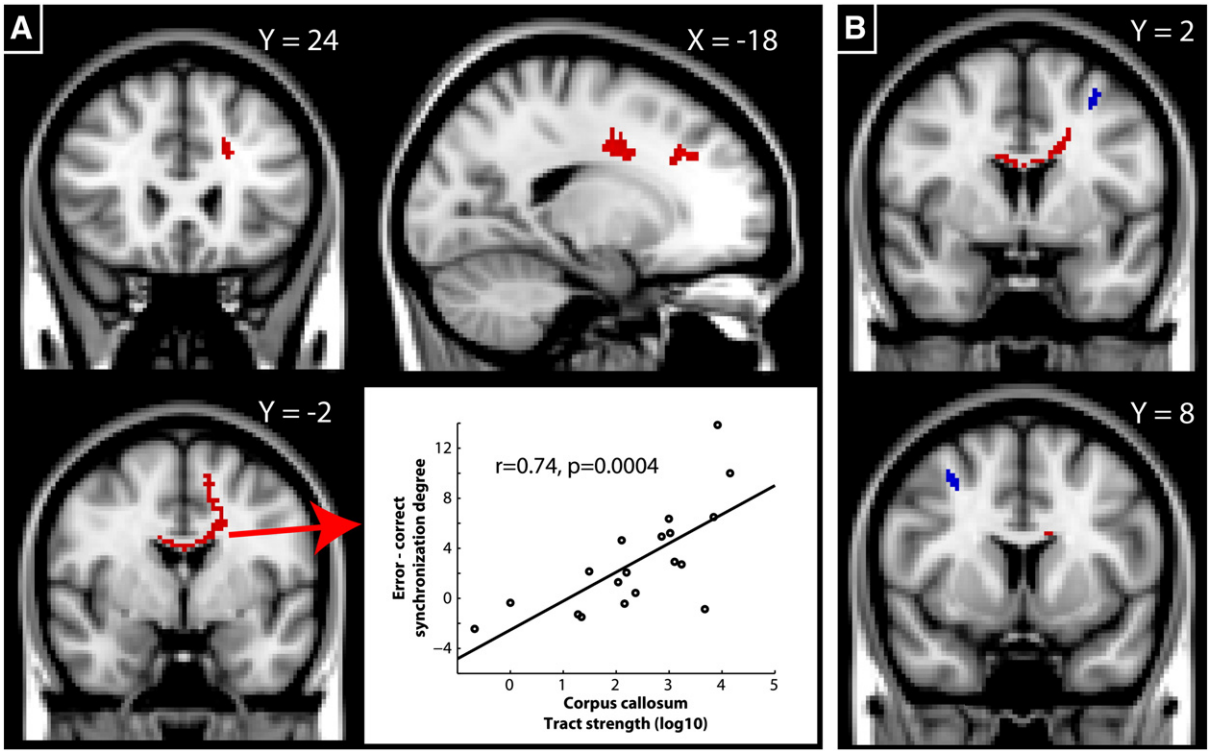

Fig. 8. Subjects in whom FCz (medial frontal electrode) was a stronger "hub" for cortico-cortical functional connectivity had stronger white matter tracks linking the error-theta dipole source (A) to the corpus callosum and white matter in the superior frontal cortex. Scatter plot shows the relationship across subjects for the voxels in the corpus callosum. Panel (B) shows the results from the IC-dipole (in blue).

In contrast to the robust correlations between tract strength and electrophysiological activity, no correlations were observed between tract strength and task performance, measured either as overall error rate or post-error response time change. There are several possible explanations for this. First, it is possible that anatomical pathways supporting performance metrics such as error rate and post-error behavior adaptations are at least slightly different from those that generate the medial frontal theta response to errors. Second, it is possible that this theta-related pathway is more involved in other adjustments that are not reflected in error rate or post-error reaction time adjustment, such as increased activity in lateral prefrontal cortex or increased physiological arousal. Indeed, medial frontal error dynamics are not always correlated with simple performance measures such as those used here. For example, patients with obsessive–compulsive disorder, and healthy students who score high on measures of obsessive–compulsive disorder, are not different from control subjects in terms of performance on cognitive control tasks such as that used here, but do show an aberrant medial frontal error-related negativity (Gehring et al., 2000; Grundler et al., 2009). Even within young healthy student samples, error-related EEG activity sometimes (e.g., Gehring et al., 1993; Ridderinkhof et al., 2003), but not always (e.g., Gehring and Fencsik, 2001) correlates with post-error behavioral performance. Taken together, previous and the current findings suggest that the neural networks supporting task performance on such cognitive control tasks may only partly overlap with neural networks that directly drive the error-related medial frontal electrophysiological response.

Tract strength is a statistical measure of connectivity, and it remains unclear precisely what micro- and mesoscopic-level biological properties contribute to tract strength. However, empirically observed correlations with behavior (Cohen et al., 2009c; Forstmann et al., 2010), functional MRI-based functional connectivity (Cohen et al., 2008a), and the present analyses provide evidence in favor of tract strength reflecting a meaningful and informative aspect of brain connectivity. Indeed, results from this study–particularly the link between synchronization degree and corpus callosal connectivity strength–are consistent with the idea that tract strength measures, at least in part, the efficiency with which information can transmit among spatially distant brain regions.

Independent component vs. theta-band power

The selection of an independent component from each subject was based on the component topography, which was similar to the error-correct theta-band power (Fig. 2). Remarkably, the time–frequency characteristics were also similar to that of the observed and also CSD data (Fig. 3).

Not surprisingly, the IC-dipole explained more of the independent component variance compared to the amount of theta topographical variance explained by the theta-dipole. Indeed, the independent component is a topographical weighting reflecting maximally temporally independent EEG dynamics, whereas the theta-band power topography is simply the observed data filtered from 4 to 8 Hz. Nonetheless, the analyses in which dipole-seeded tractography was correlated with EEG dynamics showed mainly similarities between the theta-dipole seed and the IC-dipole seed, suggesting that these correlations reveal brain structure–function links that are robust to the precise analysis approach. Indeed, most of the differences between analysis approaches were relatively minor and related to the precise anatomical location (see Figs. 7 and 8) or statistical significance level (e.g., the IC-dipole analysis showed a correlation in the corpus callosum with a p-value less than .05 but greater than the map-wise threshold). The biggest difference was the lack of significance in the ventral striatum in the IC-dipole analysis; it is possible that the dipole based on the observed theta topography is more sensitive to the "error processing" network as a whole, also considering the correlation results were more robust for the theta-dipole approach.

Conclusions

Results from this investigation provide novel evidence for the neuroanatomical networks underlying the generation of medial frontal error-related neural dynamics. These findings also add to a growing literature demonstrating the usefulness of diffusion-weighted imaging and diffusion-based white matter fiber tractography in elucidating neural networks that support cognitive processes. Still, much remains to be discovered about these networks, including: the precise functional contribution of the striatal and frontal areas that showed significant connectivity–activity correlations; how these anatomical pathways might constrain the efficacy of neurochemical signaling such as dopamine and norepinephrine, which have been implicated in action/error monitoring (Jocham and Ullsperger, 2009) and relies on long-range white matter connections; and whether and how these pathways may be shaped by experience, time, or training.

Acknowledgments

MXC is supported by a Vidi grant from the Netherlands Organization for Scientific Research (NWO). The author thanks Irene van de Vijver for assistance with the task and piloting, Jessika Buitenweg for assistance with MRI and EEG data collection, James F Cavanagh for assistance with MRI preprocessing, and Heleen Slagter for critical comments on the manuscript.

References

Amodio, D.M., Jost, J.T., Master, S.L., Yee, C.M., 2007. Neurocognitive correlates of liberalism and conservatism. Nat Neurosci 10, 1246–1247.
Aron, A.R., Behrens, T.E., Smith, S., Frank, M.J., Poldrack, R.A., 2007. Triangulating a cognitive control network using diffusion-weighted magnetic resonance imaging (MRI) and functional MRI. J Neurosci 27, 3743–3752.
Bates, A.T., Kiehl, K.A., Laurens, K.R., Liddle, P.F., 2009. Low-frequency EEG oscillations associated with information processing in schizophrenia. Schizophr Res 115, 222–230.
Behrens, T.E., Berg, H.J., Jbabdi, S., Rushworth, M.F., Woolrich, M.W., 2007. Probabilistic diffusion tractography with multiple fibre orientations: what can we gain? Neuroimage 34, 144–155.
Cavanagh, J.F., Cohen, M.X., Allen, J.J., 2009. Prelude to and resolution of an error: EEG phase synchrony reveals cognitive control dynamics during action monitoring. J Neurosci 29, 98–105.
Christie, G.J., Tata, M.S., 2009. Right frontal cortex generates reward-related theta-band oscillatory activity. Neuroimage 48, 415–422.
Cohen, M.X., Elger, C.E., Ranganath, C., 2007. Reward expectation modulates feedback-related negativity and EEG spectra. Neuroimage 35, 968–978.
Cohen, M.X., Elger, C.E., Weber, B., 2008a. Amygdala tractography predicts functional connectivity and learning during feedback-guided decision-making. Neuroimage 39, 1396–1407.
Cohen, M.X., Ridderinkhof, K.R., Haupt, S., Elger, C.E., Fell, J., 2008b. Medial frontal cortex and response conflict: evidence from human intracranial EEG and medial frontal cortex lesion. Brain Res 1238, 127–142.
Cohen, M.X., Axmacher, N., Lenartz, D., Elger, C.E., Sturm, V., Schlaepfer, T.E., 2009a. Neuroelectric signatures of reward learning and decision-making in the human nucleus accumbens. Neuropsychopharmacology 34, 1649–1658.
Cohen, M.X., Axmacher, N., Lenartz, D., Elger, C.E., Sturm, V., Schlaepfer, T.E., 2009b. Nuclei accumbens phase synchrony predicts decision-making reversals following negative feedback. J Neurosci 29, 7591–7598.
Cohen, M.X., Schoene-Bake, J.C., Elger, C.E., Weber, B., 2009c. Connectivity-based segregation of the human striatum predicts personality characteristics. Nat Neurosci 12, 32–34.
Cohen, M.X., van Gaal, S., Ridderinkhof, K.R., Lamme, V.A., 2009d. Unconscious errors enhance prefrontal–occipital oscillatory synchrony. Front Hum Neurosci 3, 54.
Cohen, M.X., Bour, L., Mantione, M., Figee, M., vinck, M., Tijssen, M.A.J., van Rootselaar, F., van den Munckhof, P., Schuurman, P.R., Denys, D., in press. Top-down directed synchrony from medial frontal cortex to nucleus accumbens during reward anticipation. Hum Brain Mapp.
Danielmeier, C., Wessel, J.R., Ullsperger, M., 2010. The Structural Basis of Error Awareness. Poster presented at Organization for Human Brain Mapping conference, Barcelona.
Debener, S., Ullsperger, M., Siegel, M., Fiehler, K., von Cramon, D.Y., Engel, A.K., 2005. Trial-by-trial coupling of concurrent electroencephalogram and functional magnetic resonance imaging identifies the dynamics of performance monitoring. J Neurosci 25, 11730–11737.
Delorme, A., Makeig, S., 2004. EEGLAB: an open source toolbox for analysis of single-trial EEG dynamics including independent component analysis. J Neurosci Methods 134, 9–21.
Dragoi, G., Buzsaki, G., 2006. Temporal encoding of place sequences by hippocampal cell assemblies. Neuron 50, 145–157.
Egner, T., Hirsch, J., 2005a. Cognitive control mechanisms resolve conflict through cortical amplification of task-relevant information. Nat Neurosci 8, 1784–1790.
Egner, T., Hirsch, J., 2005b. The neural correlates and functional integration of cognitive control in a Stroop task. Neuroimage 24, 539–547.
Falkenstein, M., Hoormann, J., Christ, S., Hohnsbein, J., 2000. ERP components on reaction errors and their functional significance: a tutorial. Biol Psychol 51, 87–107.
Forstmann, B.U., Jahfari, S., Scholte, H.S., Wolfensteller, U., van den Wildenberg, W.P., Ridderinkhof, K.R., 2008. Function and structure of the right inferior frontal cortex predict individual differences in response inhibition: a model-based approach. J Neurosci 28, 9790–9796.
Forstmann, B.U., Anwander, A., Schafer, A., Neumann, J., Brown, S., Wagenmakers, E.J., Bogacz, R., Turner, R., 2010. Cortico-striatal connections predict control over speed and accuracy in perceptual decision making. Proc Natl Acad Sci USA 107, 15916–15920.
Gehring, W.J., Fencsik, D.E., 2001. Functions of the medial frontal cortex in the processing of conflict and errors. J Neurosci 21, 9430–9437.
Gehring, W.J., Knight, R.T., 2000. Prefrontal–cingulate interactions in action monitoring. Nat Neurosci 3, 516–520.
Gehring, W.J., Goss, B., Coles, M.G., Meyer, D.E., Donchin, E., 1993. A neural system for error detection and compensation. Psychol Sci 4, 385–390.
Gehring, W.J., Himle, J., Nisenson, L.G., 2000. Action-monitoring dysfunction in obsessive–compulsive disorder. Psychol Sci 11, 1–6.
Grundler, T.O., Cavanagh, J.F., Figueroa, C.M., Frank, M.J., Allen, J.J., 2009. Task-related dissociation in ERN amplitude as a function of obsessive–compulsive symptoms. Neuropsychologia 47, 1978–1987.
Haber, S.N., Kunishio, K., Mizobuchi, M., Lynd-Balta, E., 1995. The orbital and medial prefrontal circuit through the primate basal ganglia. J Neurosci 15, 4851–4867.
Hanslmayr, S., Pastotter, B., Bauml, K.H., Gruber, S., Wimber, M., Klimesch, W., 2008. The electrophysiological dynamics of interference during the Stroop task. J Cogn Neurosci 20, 215–225.
Hogan, A.M., Vargha-Khadem, F., Saunders, D.E., Kirkham, F.J., Baldeweg, T., 2006. Impact of frontal white matter lesions on performance monitoring: ERP evidence for cortical disconnection. Brain 129, 2177–2188.
Holroyd, C.B., Coles, M.G., 2002. The neural basis of human error processing: reinforcement learning, dopamine, and the error-related negativity. Psychol Rev 109, 679–709.
Huerta, P.T., Lisman, J.E., 1995. Bidirectional synaptic plasticity induced by a single burst during cholinergic theta oscillation in CA1 in vitro. Neuron 15, 1053–1063.
Jensen, O., Lisman, J.E., 2000. Position reconstruction from an ensemble of hippocampal place cells: contribution of theta phase coding. J Neurophysiol 83, 2602–2609.
Jocham, G., Ullsperger, M., 2009. Neuropharmacology of performance monitoring. Neurosci Biobehav Rev 33, 48–60.
Kasanetz, F., Riquelme, L.A., O'Donnell, P., Murer, M.G., 2006. Turning off cortical ensembles stops striatal up states and elicits phase perturbations in cortical and striatal slow oscillations in rat in vivo. J Physiol 577, 97–113.
Kayser, J., Tenke, C.E., 2006. Principal components analysis of Laplacian waveforms as a generic method for identifying ERP generator patterns: I. evaluation with auditory oddball tasks. Clin Neurophysiol 117, 348–368.
Kerns, J.G., Cohen, J.D., MacDonald 3rd, A.W., Cho, R.Y., Stenger, V.A., Carter, C.S., 2004. Anterior cingulate conflict monitoring and adjustments in control. Science 303, 1023–1026.
Khader, P.H., Jost, K., Ranganath, C., Rösler, F., 2010. Theta and alpha oscillations during working-memory maintenance predict successful long-term memory encoding. Neurosci Lett 468, 339–343.
King, J.A., Korb, F.M., von Cramon, D.Y., Ullsperger, M., 2010. Post-error behavioral adjustments are facilitated by activation and suppression of task-relevant and task-irrelevant information processing. J Neurosci 30, 12759–12769.
Larson, M.J., Fair, J.E., Good, D.A., Baldwin, S.A., 2010. Empathy and error processing. Psychophysiology 47, 415–424.
Luu, P., Tucker, D.M., 2001. Regulating action: alternating activation of midline frontal and motor cortical networks. Clin Neurophysiol 112, 1295–1306.
Marco-Pallares, J., Cucurell, D., Cunillera, T., Garcia, R., Andres-Pueyo, A., Münte, T.F., Rodriguez-Fornells, A., 2008. Human oscillatory activity associated to reward processing in a gambling task. Neuropsychologia 46, 241–248.
Mathalon, D.H., Whitfield, S.L., Ford, J.M., 2003. Anatomy of an error: ERP and fMRI. Biol Psychol 64, 119–141.
Mazaheri, A., Nieuwenhuis, I.L., van Dijk, H., Jensen, O., 2009. Prestimulus alpha and mu activity predicts failure to inhibit motor responses. Hum Brain Mapp 30, 1791–1800.
Micheloyannis, S., Pachou, E., Stam, C.J., Breakspear, M., Bitsios, P., Vourkas, M., Erimaki, S., Zervakis, M., 2006. Small-world networks and disturbed functional connectivity in schizophrenia. Schizophr Res 87, 60–66.
Miltner, W.H., Lemke, U., Weiss, T., Holroyd, C., Scheffers, M.K., Coles, M.G., 2003. Implementation of error-processing in the human anterior cingulate cortex: a source analysis of the magnetic equivalent of the error-related negativity. Biol Psychol 64, 157–166.
Montaron, M.F., Deniau, J.M., Menetrey, A., Glowinski, J., Thierry, A.M., 1996. Prefrontal cortex inputs of the nucleus accumbens-nigro-thalamic circuit. Neuroscience 71, 371–382.
Morris, S.E., Yee, C.M., Nuechterlein, K.H., 2006. Electrophysiological analysis of error monitoring in schizophrenia. J Abnorm Psychol 115, 239–250.
Münte, T.F., Heldmann, M., Hinrichs, H., Marco-Pallares, J., Krämer, U.M., Sturm, V., Heinze, H.J., 2007. Nucleus accumbens is involved in human action monitoring: evidence from invasive electrophysiological recordings. Front Hum Neurosci 1, 11.

Olvet, D.M., Hajcak, G., 2008. The error-related negativity (ERN) and psychopathology: toward an endophenotype. Clin Psychol Rev 28, 1343–1354.
Onton, J., Delorme, A., Makeig, S., 2005. Frontal midline EEG dynamics during working memory. Neuroimage 27, 341–356.
Palva, S., Monto, S., Palva, J.M., 2010. Graph properties of synchronized cortical networks during visual working memory maintenance. Neuroimage 49, 3257–3268.
Potts, G.F., George, M.R., Martin, L.E., Barratt, E.S., 2006. Reduced punishment sensitivity in neural systems of behavior monitoring in impulsive individuals. Neurosci Lett 397, 130–134.
Ridderinkhof, K.R., Nieuwenhuis, S., Bashore, T.R., 2003. Errors are foreshadowed in brain potentials associated with action monitoring in cingulate cortex in humans. Neurosci Lett 348, 1–4.
Ridderinkhof, K.R., Ullsperger, M., Crone, E.A., Nieuwenhuis, S., 2004. The role of the medial frontal cortex in cognitive control. Science 306, 443–447.
Rushworth, M.F., Buckley, M.J., Behrens, T.E., Walton, M.E., Bannerman, D.M., 2007. Functional organization of the medial frontal cortex. Curr Opin Neurobiol 17, 220–227.
Sauseng, P., Griesmayr, B., Freunberger, R., Klimesch, W., 2010. Control mechanisms in working memory: a possible function of EEG theta oscillations. Neurosci Biobehav Rev 34, 1015–1022.
Srinivasan, R., Winter, W.R., Ding, J., Nunez, P.L., 2007. EEG and MEG coherence: measures of functional connectivity at distinct spatial scales of neocortical dynamics. J Neurosci Methods 166, 41–52.
Stam, C.J., Jones, B.F., Nolte, G., Breakspear, M., Scheltens, P., 2007. Small-world networks and functional connectivity in Alzheimer's disease. Cereb Cortex 17, 92–99.
Stemmer, B., Segalowitz, S.J., Witzke, W., Schonle, P.W., 2004. Error detection in patients with lesions to the medial prefrontal cortex: an ERP study. Neuropsychologia 42, 118–130.
Swick, D., Turken, A.U., 2002. Dissociation between conflict detection and error monitoring in the human anterior cingulate cortex. Proc Natl Acad Sci USA 99, 16354–16359.
Teipel, S.J., Pogarell, O., Meindl, T., Dietrich, O., Sydykova, D., Hunklinger, U., Georgii, B., Mulert, C., Reiser, M.F., Moller, H.J., Hampel, H., 2009. Regional networks underlying interhemispheric connectivity: an EEG and DTI study in healthy ageing and amnestic mild cognitive impairment. Hum Brain Mapp 30, 2098–2119.
Trujillo, L.T., Allen, J.J., 2007. Theta EEG dynamics of the error-related negativity. Clin Neurophysiol 118, 645–668.
Tsujimoto, T., Shimazu, H., Isomura, Y., 2006. Direct recording of theta oscillations in primate prefrontal and anterior cingulate cortices. J Neurophysiol 95, 2987–3000.
Tsujimoto, T., Shimazu, H., Isomura, Y., Sasaki, K., 2010. Theta oscillations in primate prefrontal and anterior cingulate cortices in forewarned reaction time tasks. J Neurophysiol 103, 827–843.
Ullsperger, M., von Cramon, D.Y., 2006. The role of intact frontostriatal circuits in error processing. J Cogn Neurosci 18, 651–664.
Ullsperger, M., von Cramon, D.Y., Muller, N.G., 2002. Interactions of focal cortical lesions with error processing: evidence from event-related brain potentials. Neuropsychology 16, 548–561.
van Veen, V., Carter, C.S., 2002. The anterior cingulate as a conflict monitor: fMRI and ERP studies. Physiol Behav 77, 477–482.
Vlamings, P.H., Jonkman, L.M., Hoeksma, M.R., van Engeland, H., Kemner, C., 2008. Reduced error monitoring in children with autism spectrum disorder: an ERP study. Eur J Neurosci 28, 399–406.
Vocat, R., Pourtois, G., Vuilleumier, P., 2008. Unavoidable errors: a spatio-temporal analysis of time-course and neural sources of evoked potentials associated with error processing in a speeded task. Neuropsychologia 46, 2545–2555.
Wang, C., Ulbert, I., Schomer, D.L., Marinkovic, K., Halgren, E., 2005. Responses of human anterior cingulate cortex microdomains to error detection, conflict monitoring, stimulus-response mapping, familiarity, and orienting. J Neurosci 25, 604–613.
Westlye, L.T., Walhovd, K.B., Bjornerud, A., Due-Tonnessen, P., Fjell, A.M., 2009. Error-related negativity is mediated by fractional anisotropy in the posterior cingulate gyrus—a study combining diffusion tensor imaging and electrophysiology in healthy adults. Cereb Cortex 19, 293–304.
Winter, W.R., Nunez, P.L., Ding, J., Srinivasan, R., 2007. Comparison of the effect of volume conduction on EEG coherence with the effect of field spread on MEG coherence. Stat Med 26, 3946–3957.
Womelsdorf, T., Johnston, K., Vinck, M., Everling, S., 2010. Theta-activity in anterior cingulate cortex predicts task rules and their adjustments following errors. Proc Natl Acad Sci USA 107, 5248–5253.
Zaehle, T., Herrmann, C.S., 2011. Neural synchrony and white matter variations in the human brain — relation between evoked gamma frequency and corpus callosum morphology. Int J Psychophysiol 79, 49–54.